Myosin VI Walks "Wiggly" on Actin with Large and Variable Tilting

Yujie Sun,[1] Harry W. Schroeder III,[1] John F. Beausang,[1] Kazuaki Homma,[2] Mitsuo Ikebe,[2] and Yale E. Goldman[1,*]
[1]Pennsylvania Muscle Institute, University of Pennsylvania, Philadelphia, PA 19104, USA
[2]University of Massachusetts Medical School, North Worcester, MA 01655, USA
*Correspondence: goldmany@mail.med.upenn.edu

SUMMARY

Myosin VI is an unconventional motor protein with unusual motility properties such as its direction of motion and path on actin and a large stride relative to its short lever arms. To understand these features, the rotational dynamics of the lever arm were studied by single-molecule polarized total internal reflection fluorescence (polTIRF) microscopy during processive motility of myosin VI along actin. The axial angle is distributed in two peaks, consistent with the hand-over-hand model. The changes in lever arm angles during discrete steps suggest that it exhibits large and variable tilting in the plane of actin and to the sides. These motions imply that, in addition to the previously suggested flexible tail domain, there is a compliant region between the motor domain and lever arm that allows myosin VI to accommodate the helical position of binding sites while taking variable step sizes along the actin filament.

INTRODUCTION

Myosin VI is an unconventional motor protein of the myosin superfamily that serves as an anchor and transporter in cellular processes such as vesicular membrane traffic, cell migration, and mitosis (Buss et al., 2004; Cramer, 2000; Frank et al., 2004; Hasson, 2003; Sweeney and Houdusse, 2007). Similar to other myosins, the myosin VI heavy chain is composed of an N-terminal motor domain that binds actin and ATP, a calmodulin (CaM) binding region, and an α-helical domain leading to the cargo binding region (Hasson and Mooseker, 1994). One CaM subunit is bound very tightly to a peptide sequence unique to myosin VI, and a second CaM is bound to a consensus CaM binding IQ domain (Bahloul et al., 2004; Morris et al., 2003). The motility of myosin VI exhibits several unusual properties that have made it the subject of many structural (Ménétrey et al., 2005, 2007; Wells et al., 1999) and single-molecule (Ali et al., 2004; Altman et al., 2004; Balci et al., 2005; Iwaki et al., 2006; Nishikawa et al., 2002; Ökten et al., 2004; Park et al., 2006; Rock et al., 2001, 2005; Yildiz et al.,

2004; Yildiz and Selvin, 2005) investigations. It has been shown that myosin VI moves processively in a hand-over-hand manner toward the minus end of actin filaments, opposite to other classes of myosin. The reported measurements of myosin VI step size range between 25 and 36 nm with high variability (e.g., ± ~12 nm; Rock et al., 2001). Ali et al. (2004) have shown with an experimental geometry that avoids surface hindrance that full-length dimeric myosin VI carries bead cargos either straight along actin or on a right-handed spiral, suggesting an average step size even larger than 36 nm.

Another well-studied dimeric processive motor, myosin V, also exhibits hand-over-hand processive motility with a tightly distributed 36 nm stride. Myosin V contains six CaM or CaM-like subunits on each of its lever arms, giving these structures enough length (~24 nm each) for the two heads to bind simultaneously to actin monomers separated along the filament by 36 nm (Cheney et al., 1993; Forkey et al., 2003; Mehta et al., 1999). Only limited distortion of the structure is observed in EMs of myosin V bound to two actin monomers separated by this distance (Walker et al., 2000) and the two heavy chains join to form a strong coiled-coil α helix at a head-stalk junction just beyond the IQ motifs (Hasson and Mooseker, 1994; Mehta et al., 1999). For myosin VI, on the other hand, the two CaM subunits would give, at most, a 7.2 nm length of lever arm, not sufficient for the dimeric molecule to span over 25–36 nm without substantial structural rearrangements. A C-terminal extension of the heavy chain has been suggested to increase the lever arm length to 10 nm (Rock et al., 2005). It has been puzzling how myosin VI achieves the large step size in spite of its short lever arm. The proximal tail domain (PTD) has been suggested to unwind to allow the molecule to stretch out to span over the filament distance of its stride (Altman et al., 2004; Ökten et al., 2004; Rock et al., 2005; Yildiz et al., 2004). This idea, though, introduces the problem that a random segment of sequence would not support a mechanical load, whereas optical trap experiments indicate that myosin VI can exert up to 2 pN without slowing (Altman et al., 2004).

Debate has also taken place over whether myosin VI is monomeric or dimeric in vivo. Expressed native myosin VI is a nonprocessive monomer (Lister et al., 2004), whereas artificially dimerized myosin VI shows robust processivity (Ökten et al., 2004; Yildiz et al., 2004). Native myosin VI monomers may dimerize via clustering through their cargo

binding domain, and these dimers behave similarly to the artificially dimerized myosin VI and show processive movement (Park et al., 2006). Monomeric myosin VI also moves processively when it binds cargo (Iwaki et al., 2006).

As with other myosins, rotations, tilting, and twisting of the functional domains are expected to be essential motions of myosin VI. In myosin V and II, for instance, a rotational stroke of the lever arm, within the axial plane containing the actin filament, is the main structural change that moves the cargo (Forkey et al., 2003; Howard, 1997; Purcell et al., 2002; Tyska and Warshaw, 2002; Yildiz et al., 2003). Out-of-plane motions are used by myosin V to alter its path, possibly to avoid obstacles on its track (Syed et al., 2006). For myosin VI, if the PTD is flexible, then the azimuthal angle of the myosin VI lever arm around the actin filament and the path of the molecule are expected to be very variable.

In the present work, we used single-molecule polarized total internal reflection fluorescence microscopy (polTIRF) (Forkey et al., 1999, 2000, 2003; Rosenberg et al., 2005) to measure angular changes of fluorescent-labeled CaM in the myosin VI lever arm domain. A short smooth muscle myosin II coiled-coil region attached to the tail domain of myosin VI (Nishikawa et al., 2002) ensured dimerization of the coiled-coil domain of myosin VI, leading to robust processivity. Large tilting motions, expected from the lever arm model, were detected at the rate of stepping. The azimuthal angle changes of the leading and trailing lever arms suggest that, in addition to walking straight, myosin VI often steps left and right around an actin filament. The large variability of angle, accompanied by large tilting and twisting motions outside of the actin axial plane, explains the high variability of myosin VI step size and implies that there is a compliant region near the head-lever arm junction.

RESULTS

Recordings of Single-Molecule PolTIRF Data

The single-molecule polTIRF setup was described previously (Forkey et al., 2005; Rosenberg et al., 2005). Briefly, bifunctional rhodamine (BR) probes in myosin VI molecules bound to actin were excited by polarized evanescent waves generated by total internal reflection (TIR) microscopy. The polarized fluorescent emission from single rhodamine probes was used to determine its orientation in terms of its axial angle (β) relative to the actin filament, the azimuthal angle (α) around the actin filament, and the amplitude of μs wobbling (δ_s). In the present work, and described more fully elsewhere (Beausang et al., 2007), eight combinations of time-multiplexed incident directions and polarizations (s, p, 45° and 135° polarizations in both incident beams) allow unambiguous 3D resolution of individual probe dipole orientations within a hemisphere during each 80 ms detection cycle. See the Experimental Procedures and Figure S1, available online, for definitions of the excitation paths and polarizations. The remaining
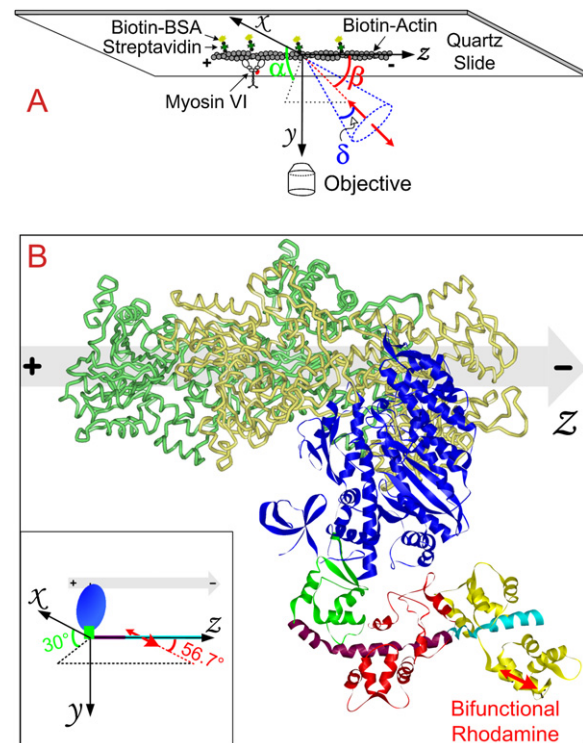
Figure 1. The Definition of the Coordinate Frame Relative to Actin

(A) Cartesian axes and Euler angles of the single-molecule polTIRF assay. Actin filaments were immobilized on the lower surface of the quartz slide via biotin-streptavidin linkage. The actin pointed (−) end is used to define the actin coordinate frame. β is the probe axial angle relative to the actin filament, and α is the azimuthal angle of the probe around the actin filament relative to the x axis. δ is the half angle of the wobble cone, which describes the restricted wobbling motion of the probe and protein domain.

(B) The orientation of the bifunctional rhodamine (BR) probe relative to the actin. The myosin VI molecule in the nucleotide-free state was docked onto actin by aligning the motor domain with that of myosin II in the actomyosin near-rigor complex. Blue, motor domain; green ribbons, converter domain; purple, special insert; cyan, IQ domain; red, tightly bound CaM; yellow, IQ-bound CaM; and green tubes, actin monomers. The red double-headed arrow shows the position of the BR probe attached to residues 66 and 73 of the CaM. The lower end of the dipole is pointing out of the page. The azimuthal angle of the probe is at −60° relative to the azimuthal position of the motor domain. When the motor domain is on the bottom of the actin (on the y axis) as in the figure, the probe's azimuthal angle in the actin coordinate frame is therefore 30° (inset).

ambiguity is due to the dipolar nature of the fluorescent probe. The coordinate frame of Figure 1A is defined relative to actin, with the z axis pointing in the direction of motility, the pointed (−) end of actin for myosin VI. Because actin filaments are attached firmly to the slides in the experimental assay, myosin VI most likely binds and walks on an actin filament in the hemispherical space that faces the objective ($0 < \beta_{lever} < 180°$ and $0° < \alpha_{lever} < 180°$, Figure 1). Given that assumption, the appropriate hemisphere defining the corresponding range of probe angles is tilted by the
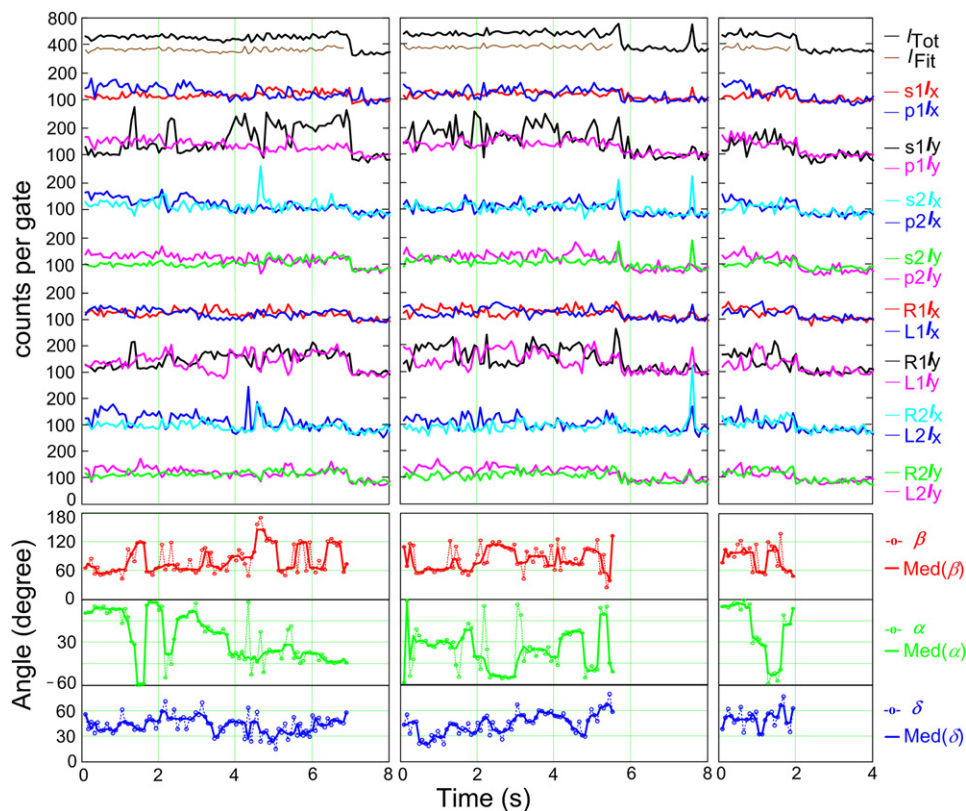
Figure 2. Typical Single-Molecule PolTIRF Recordings and Fitted Angles of Myosin VI during Processive Motility at 150 μM ATP

Top panels are the 16 fluorescence intensities detected by the two APDs. L and R denote the 45° and 135° polarization excitation, respectively. The total intensity (top-most black trace, I_{Tot}) is a weighted sum of all intensities. The bottom panels show the angles obtained from fitting of the wobble-cone model of the probe fluorescence to the 16 intensities. In the angle traces, the dashed lines connecting open circles are the angle values from fitting, and the solid curves are angle values smoothed by a median filter with a window size of 5, as denoted by Med(angle).

relative angle between the myosin VI molecule and the probe, defined by its two linked Cys residues. Using the available crystal structure of myosin VI (Ménétrey et al., 2005) docked onto actin (Figure 1B) by superimposing it onto that of myosin II in the actomyosin near-rigor complex (Rayment et al., 1993), the azimuthal angle of the probe relative to that of the bound actin monomer is approximately −60°. Thus, the probe hemisphere corresponding to exclusion of the myosin VI lever from the glass slide is given by $0 < \beta_{probe} < 180°$ and $-60° < \alpha_{probe} < 120°$. One end of the probe dipole remains in this hemisphere as the lever arm rotates, and the other end is restricted to the opposite hemisphere.

Figure 2 shows three typical traces from single-molecule polTIRF experiments on myosin VI at 150 μM ATP. In each figure, the top panel shows the 16 polarized fluorescence intensities from the eight time-multiplexed incident polarizations detected by the two avalanche photodiodes (APDs). The BR probe photobleached to the background level at 7, 6, and 2 s. The bottom panels show the angles obtained from fitting a wobble-cone model of the probe fluorescence to the 16 intensities. Sample traces recorded at 500 μM ATP are given in

Figure S2. Most (>95%) of the β (red) traces from processively stepping myosin VI molecules showed clear alternating up and down transitions, the lever arm tilting characteristic of hand-over-hand stepping. The azimuthal angle (α, green traces) often, but not exclusively, changed value at the same time as β, indicating large azimuthal swaying. The μs wobble (δ_s, bottom blue traces) varied, apparently randomly, between 30° and 60°.

Kinetics

Angular transitions were picked manually from the median-filtered (window size = five samples) β traces, taking the approximate angular resolution of the measurement (10°) as a lower limit for selecting steps and avoiding spikes of the traces that deflected β for only one measurement cycle (see Figure 2). We also applied an automated step-finding algorithm (Kerssemakers et al., 2006) to select transitions in the α and β traces, and the steps were very similar to those selected manually (see Figure S2). The distributions of dwell times (Figure S3) were fitted with a kinetic model having two reaction steps: a first-order step (k_1, presumably ADP release from the trailing head) and subsequent ATP binding (k_2), to obtain
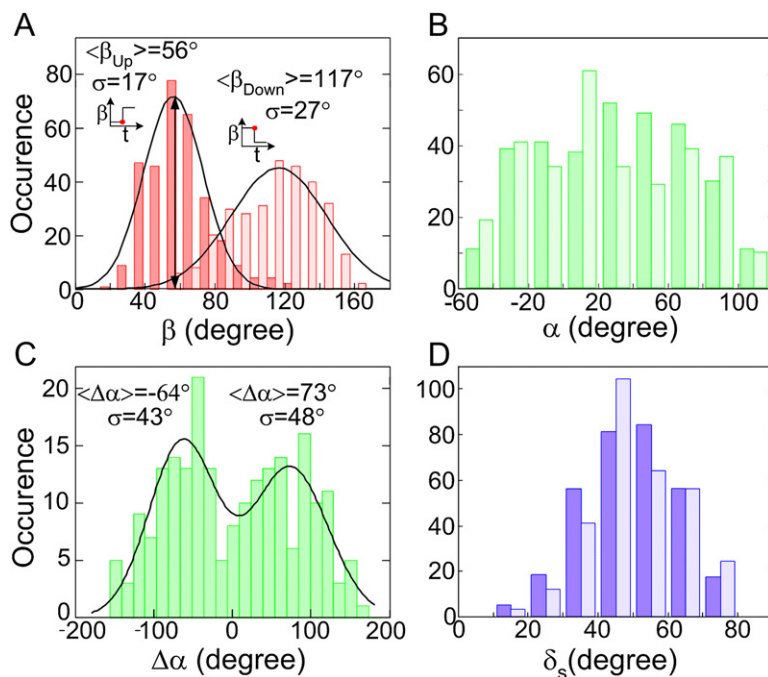
Figure 3. Distributions of the Probe Angles at Up-β Transitions and Down-β Transitions

(A) Histogram of β angles at up-β transitions (darker bars) and down-β transitions (lighter bars). The double-headed arrow denotes the estimated β angle when the labeled lever is in trailing position (see Discussion for details).
(B) Histogram of α angles at up- and down-β transitions.
(C) Histogram of the azimuthal angular change per step ($\Delta\alpha$).
(D) Histogram of δ_s angles at up- and down-β transitions.

apparent rate constants for the motility process. Simultaneous fitting of the dwell times at 150 and 500 μM ATP gave $k_1 = 9.84$ s^{-1} and $k_2 = 0.019$ μM^{-1}s^{-1}, similar to other reported values (Altman et al., 2004; De La Cruz et al., 2001; Park et al., 2006; Robblee et al., 2004; Yildiz et al., 2004). Dwell time data at ATP concentrations ranging down to 20 μM were also compatible with the two-step kinetic model. The stride length per angular transition of β can be calculated from product of the dwell time and the average velocity, which was measured as 81.7 nm/s at 150 μM ATP and 154.3 nm/s at 500 μM ATP. Thus, the amount of translocation along actin per tilt of the CaM (the apparent stride length) of myosin VI is 37 and 32 nm at 150 and 500 μM ATP, respectively.

Angular Distributions

The distributions of the probe β values just prior to upward and downward β transitions (Figure 3A) show two clear peaks. In the coordinate frame of Figure 1, the trailing head lever arm has the smaller β angle and the leading head the larger β. The peak of β at the smaller angle (56°), corresponding to the trailing head, is considerably narrower ($\sigma_{\beta\_trail} = 17°$, comparable to that of myosin II

S1; Quinlan et al., 2005) than the β peak at larger angle 117° (leading head, $\sigma_{\beta\_lead} = 27°$), suggesting that the leading head is more disordered or has a wider range of angles than the trailing head.

In contrast to the difference in width between the leading and trailing β distributions, the azimuthal probe angles around the actin filament α, measured just before upward and downward β transitions, show similar broad distributions (Figure 3B). The change of azimuthal angle per step ($\Delta\alpha$) also has large variance of 43°–48° (Figure 3C), 1.5- to 2-fold larger than that of myosin V measured under similar conditions (data not shown). The standard deviations of β_{probe} and α_{probe} angles of myosin VI bound to actin filaments in the absence of ATP (rigor probe angles) are about 8° and 12°, respectively, considerably smaller than the breadth of the distributions during stepping. Thus, myosin VI stepping involves large azimuthal variations. The δ_s distributions were the same for the leading and trailing positions as shown in Figure 3D.

The number of upward and downward transitions of β are almost equal (Table 1), consistent with the lever arm model alternating back and forth between leading and trailing positions. As shown in Figure 2, the abrupt

Table 1. Fractions of Different Types of $\Delta\beta$-$\Delta\alpha$ Correlations

β Transition	β Increase (Trailing to Leading)			β Decrease (Leading to Trailing)		
Percentage	51% (320)			49% (304)		
α change at β transition	α increase	α decrease	α no change	α increase	α decrease	α no change
Percentage	38%	39%	23%	35%	35%	30%
Median $\Delta\beta$	44	49	60	−40	−40	−55
Median $\Delta\alpha$	53	−65	0	72	−57	0
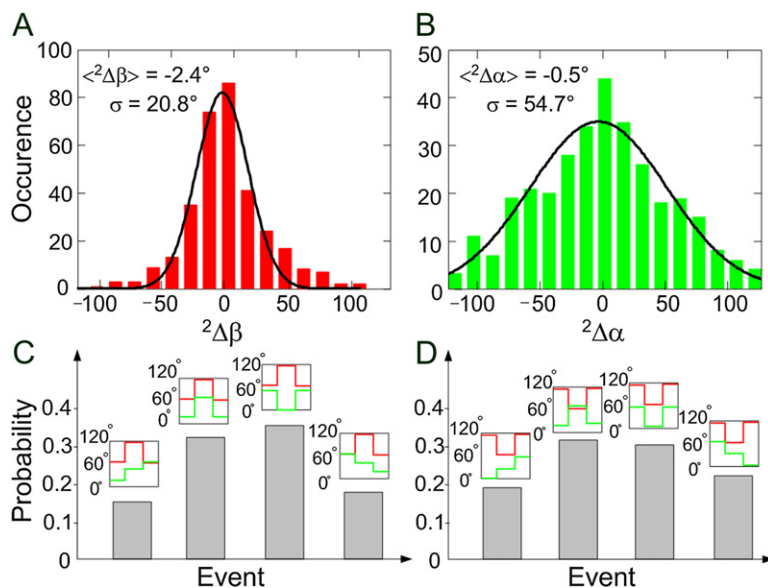
Figure 4. Distributions and Transition Probabilities for Two Successive Steps
(A) Distribution of the angle changes after two consecutive steps (same-state angular change) $^2\Delta\beta$.
(B) Distribution of $^2\Delta\alpha$.
(C and D) Probabilities and amplitudes of different $^2\Delta\alpha$ types when β goes through low-high-low transitions (C) and high-low-high transitions (D). In (C) and (D), red traces are β angles and green traces are α angles. Oppositely directed α changes are more likely on successive steps ("wiggly pattern") than two α changes in the same direction ("twirling pattern").

changes of β were often accompanied by transitions of α. At the time of β transitions, α either increased, decreased, or did not change appreciably (deflection < 10°). For both up and down β transitions, there is about an equal percentage of up, down, and null α transitions (Table 1). Thus, both the stepping head (trailing to leading position) and the nonstepping head (leading to trailing) showed large, essentially random azimuthal changes. In Table 1, $\Delta\beta$ and $\Delta\alpha$ show the differences between angles before and after the steps. For both increasing and decreasing β, the $\Delta\beta$ values were noticeably larger for transitions without any change of α ($\Delta\beta = 60°$ and $-55°$) than for ones with changes in α ($\Delta\beta = 40°-49°$). Thus, larger azimuthal motions were correlated with smaller changes of β.

If the lever arm alternates between leading and trailing positions, then it returns to its original state after two transitions, i.e., leading → trailing → leading, or trailing → leading → trailing. Because the relative orientation between labeled lever arm and the BR probe is fixed, the measured angular change of the probe after two steps, termed $^2\Delta\beta$ and $^2\Delta\alpha$, should be the same as the angular change of the lever arm, irrespective of the relative angle between the two. When $^2\Delta\alpha$ is zero or small, the molecule is walking straight along the axis of actin. Distributions of $^2\Delta\beta$ and $^2\Delta\alpha$ (Figures 4A and 4B) show that $^2\Delta\beta$ is rather narrow ($\sigma = 20.8°$), whereas $^2\Delta\alpha$ is distributed quite broadly ($\sigma = 54.7°$)—about twice as much as myosin V (data not shown). Thus myosin VI walks much more wiggly than myosin V.

Figures 4C and 4D show the proportions of different classes of $^2\Delta\alpha$ when β goes through down-up-down transitions and up-down-up transitions, respectively. In approximately two-thirds of the examples, myosin VI wiggles left and then right (or vice versa) during two consecutive steps (wiggling pattern), whereas in about one-third of the examples, it follows the same handedness over two

consecutive steps (partial twirling pattern). The fractional difference between the two stepping patterns is significant ($p < 0.05$). Thus, the likelihood for any particular azimuthal change is not completely random, but it seems to depend on the direction of the prior step.

Twirling Assay
A newly developed assay using polTIRF to monitor torque and helical motions of molecular motors detects the azimuthal rotation of sparsely labeled actin in a gliding filament assay (Beausang et al., 2006, 2007; Rosenberg et al., 2005). F-actin, sparsely labeled with tetramethyl-rhodamine at residue Cys374, actively glides on myosin bound to the microscope slide surface. In the present case, myosin VI is bound to the fused silica slide by using polylysine. The three-dimensional (3D) orientation of an individual fluorophore in the actin is monitored by polTIRF during the gliding to determine if it tracks straight or with a helical twist. In this "twirling assay," the axial angle β of the actin probe is expected to be a constant (Forkey et al., 2005; Otterbein et al., 2001; Rosenberg et al., 2005), and therefore, the appropriate hemisphere to quantify the angles for this type of experiment is the front (or rear) hemisphere relative to the direction of motility. If the filament twirls, then the azimuthal angle (α) of the actin changes steadily (Figure 5), due to a net torque exerted on it by the myosin molecules. During translocation by myosin VI, ~20% of the observed actin filaments follow a helical path with rotation around the filament axis. In those twirling filaments, myosin VI induces a right-handed twirling motion with pitch 1.3 ± 0.1 μm (mean ± SEM, n = 23).

DISCUSSION

Processive motility by two-headed dimers of myosin VI has been shown to operate by the hand-over-hand mode
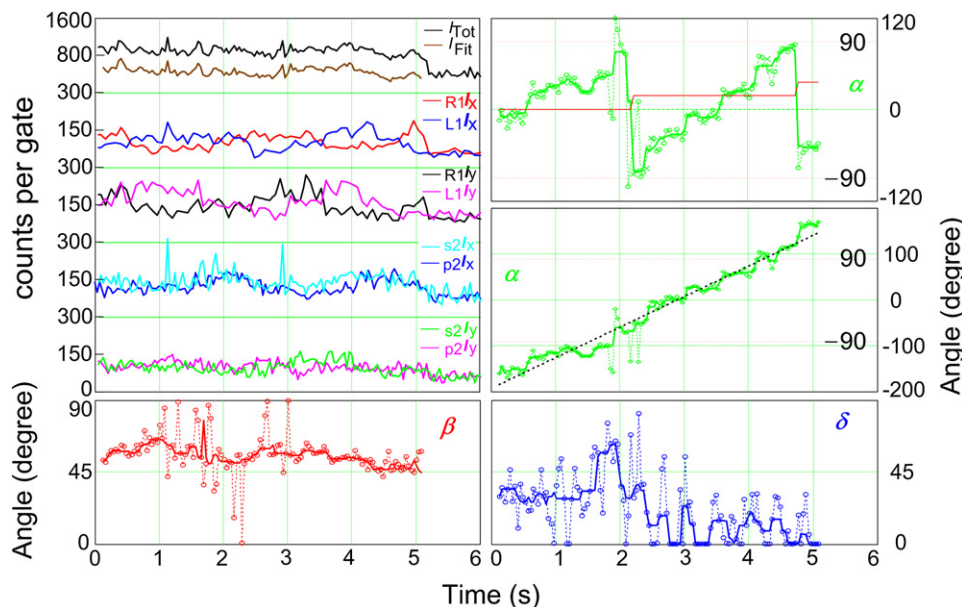
Figure 5. Typical Single-Molecule PolTIRF Recording and Fitted Angles in the Myosin VI Twirling Assay

The top left panel shows the fluorescence intensities detected by the x and y APDs for each polarized excitation light. The two bottom panels are the probe axial angle β and wobbling angle $δ_s$, respectively. The two panels on the right (green traces) are the probe azimuthal angle α. In the angle traces, open circles are the angle values from fitting and the solid curves are angle values smoothed by a median filter with a window size of five samples. In the middle right panel, angular ambiguity of α angle was corrected as follows: if there was a jump larger than a threshold of 65° in the median-filtered α trace, all data points subsequent to the jump were shifted 180° in the direction opposite to the jump, and no more than one such shift was applied in any 500 ms period. Two shifts occurred in this recording, depicted by the two steps in the red indicator trace in the top right α panel. In the resulting α trace (middle right panel), the dotted line is a linear fit giving the angular velocity. Pitch is given by the ratio of linear to angular velocity. Myosin VI induces a right-handed twirling motion around the axis of actin.

(Balci et al., 2005; Ökten et al., 2004; Yildiz et al., 2004). The biggest puzzle with myosin VI motility is its large stride, averaging 25–36 nm in various studies (Altman et al., 2004; Balci et al., 2005; Nishikawa et al., 2002; Ökten et al., 2004; Park et al., 2006; Rock et al., 2001, 2005; Yildiz et al., 2004). The length of the myosin VI putative lever arm, which contains a converter domain, a unique heavy chain insert bound to a CaM, an IQ motif with a second CaM, and possibly a rigid extension of the heavy chain, is no more than 10 nm long (Rock et al., 2005). Single-headed constructs of myosin VI produce steps of up to 18 nm, requiring postulation of a ~180° rotation of the lever arm (Bryant et al., 2007; Lister et al., 2004) and, in addition, a considerable diffusive search to complete the stride. The results presented in this paper suggest that the trajectory of the working stroke (taking place on the attached head during a step) may be highly variable for myosin VI. We used a construct containing a segment of the smooth muscle myosin II coiled-coil region attached to the tail domain of myosin VI to ensure dimerization (Nishikawa et al., 2002). The effects of the short myosin II segment on the stepping behavior of myosin VI were expected to be minimal because the motor domain, neck domain, and entire coiled-coil domain of myosin VI were preserved in the construct. The velocity, stepping rate, and ATP dependence of the motility (Nishikawa et al., 2002; Figure S3) are, in fact, consistent with results from studies on other constructs

(Park et al., 2006; Yildiz et al., 2004). The dynamic angular measurements support the previously proposed hypothesis of a large power stroke rotation of nearly 180° and also suggest that the leading head has considerable flexibility to find actin monomers over a large range of azimuthal positions. We conclude that variable motions of both the leading and trailing heads contribute to the variation of path and step size of myosin VI.

Angles of the Leading and Trailing Lever Arms

The kinetics of waiting times between β transitions over a range of ATP concentrations (Figure S3) are appropriate to the measured translocation velocities for a 30–36 nm average stride, implying that the tilting motions are associated with each step.

Because the probe is rigidly bound to CaM, which is bound tightly to the lever arm, the two peaks of β (Figure 3A) are expected to correspond to the pre- and post-power stroke orientations of the lever arm in the leading and trailing positions. Docking the myosin VI nucleotide-free crystal structure onto actin (Figure 1B) results in a lever arm that is approximately parallel to the actin filament with a probe β angle of 57° (black double-headed arrow in Figure 3A) for our bifunctional rhodamine at CaM residues 66 and 73. The peak in the β distribution at 56° is in good agreement with this angle, thus enabling assignment of this peak to the trailing (poststroke) myosin VI head.
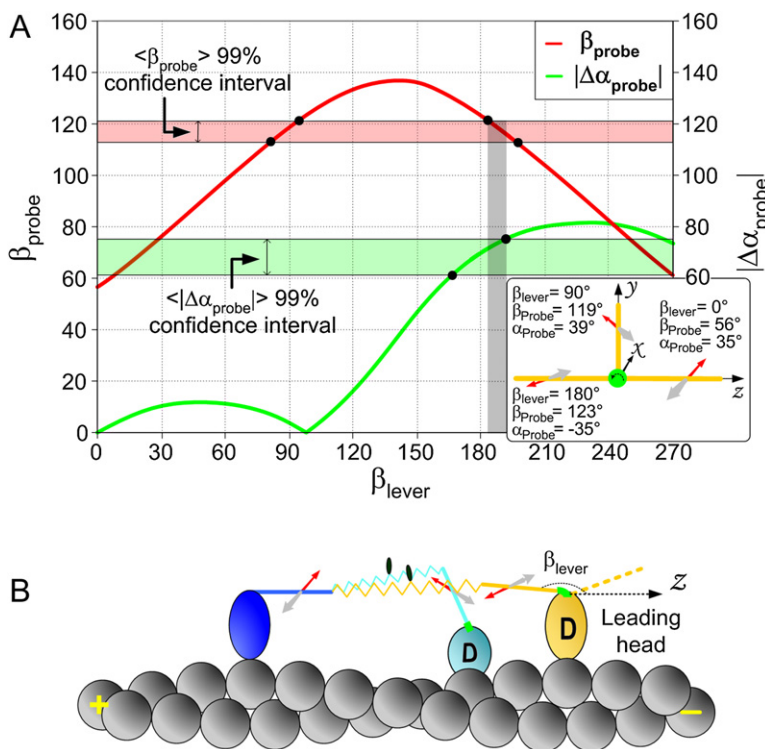
Figure 6. Lever Arm Angle Changes

(A) Predicted probe β values (β_{probe}), and the change of azimuthal probe angle ($|\Delta\alpha_{probe}|$) as the leading lever arm adopts different axial angles (β_{lever}). The inset illustrates the probe orientation when the lever arm is at axial angles of $0°$, $90°$, and $180°$ relative to the pointed end of actin filament (z axis). Between $\beta_{lever} = 0°$ and $90°$, α changes only slightly. But between $\beta_{lever} = 90°$ and $180°$, α changes much more. Yellow rods, leading lever arm; green dot, lever-head hinge. The two ends of probe dipole are differentially colored, with the red end pointing into the hemisphere used to quantify probe angles as discussed above. The 99% confidence interval of measured mean probe β angle in the leading lever arm from Figure 4A is highlighted by the red horizontal bar. The 99% confidence interval of mean azimuthal probe angular change ($|\Delta\alpha_{probe}|$) is highlighted by the green horizontal bar. The 99% confidence intervals of the mean probe angles intersect the predicted curves as denoted by black dots and overlap both confidence intervals between $\beta_{lever} = 182°$ and $190°$ as denoted by a gray vertical bar.

(B) The leading lever arm may adopt different orientations as the interhead distance changes. The blue head represents the trailing head, and the yellow and cyan ones show the leading head at different distances. The double-ended arrows represent the BR probes. The proximal tail domain and lever-head hinge in the leading head are shown as springs and pliant green segments, respectively. The black ovals on the springs represent the attachment point of the tail. At 150 μM, ATP binding is the rate-limiting step. Thus, the trailing head is mostly empty and nearly parallel to the actin filament (Ménétrey et al., 2005; Wells et al., 1999). The leading head probably contains ADP ("D"). The dashed yellow rod represents the orientation of the leading head in the ADP state if there were no load (Lister et al., 2004; Wells et al., 1999). The actual positions (solid yellow and cyan bars) depend on spacing and interhead compliance as explained in the text.

The crystal structures of the myosin VI in the prepower stroke state have been reported recently (Ménétrey et al., 2007) and suggest that the working stroke is along the axis of actin. The plane of power stroke rotation is approximately parallel to the actin filament in other myosins (Coureux et al., 2004; Dominguez et al., 1998; Smith and Rayment, 1996). Assuming this parallel motion, Figure 6A shows the predicted probe β values (β_{probe}) and the change of azimuthal probe angle ($|\Delta\alpha_{probe}|$, relative to the probe in the trailing position) as a function of the leading lever arm orientation (β_{lever}). The 99% confidence interval of measured mean β_{probe} in the leading lever arm from Figure 3A is shown as the red horizontal bar, which intersects the curve of $\beta_{leadingprobe}$ in two regions: $81°$–$94°$ and $182°$–$196°$, as denoted by the black dots in Figure 6A. These two ranges of lever arm rotation correspond, respectively, to a power stroke (approximately $L \cdot [\cos(\beta_{leadinglever}) - \cos(\beta_{trailinglever})]$. L is the length of the lever arm) along actin of $\sim$12 and $\sim$18 nm, both of which have been reported (Bryant et al., 2007; Lister et al., 2004; Rock et al., 2005). A lever arm rotation in the $81°$–$94°$ range, however, results in a very small azimuthal angular change ($<10°$, green curve in Figure 6A), which is inconsistent with the $\Delta\alpha$ distribution in Figure 3C. The green bar in Figure 6A shows the 99% confidence interval of $|\Delta\alpha_{probe}|$ during a step (data

from Figure 3C; instead of $\Delta\alpha_{probe}$, $|\Delta\alpha_{probe}|$ is used here to include both trailing-to-leading and leading-to-trailing transitions), supporting the larger powerstroke rotation with β_{lever} between $182°$ and $190°$ (gray vertical bar in Figure 6A). Therefore, our data imply that myosin VI may have a large power stroke rotation close to $180°$, as has been suggested from other studies (Bryant et al., 2007; Lister et al., 2004; Park et al., 2007). The slight mismatch between the zones of β_{lever} intersecting the 99% confidence intervals of the mean β_{probe} and $|\Delta\alpha_{probe}|$ may be due to azimuthal flexibility of myosin VI.

Note that the broader distribution of $\beta_{leadingprobe}$ than that of $\beta_{trailingprobe}$ (Figure 3A) indicates more distortion in the lever arm. Similarly, in a FIONA experiment with myosin VI, Yildiz et al. (2004) found that the fluorescent probe in the leading position had larger spatial variation than in the trailing position, suggesting an uncoupling of the lever arm from the motor head. In later work, those authors found that an engineered construct of myosin VI with the unique insert 2 removed moves in the opposite direction but with a similar step size compared for the native molecule: a result that is less favorable to the uncoupling idea (Park et al., 2007). In the present experiment, uncoupling between the lever arm and motor head would result in an increase of the wobbling motion (δ_s) of the probe in

the leading state, which was not observed (Figure 3D). Instead, we speculate that the larger variance of $\beta_{leadingprobe}$ is due to the leading lever arm adopting different orientations when it binds to different actin monomers (Figure 6B).

The most straightforward explanation of the results is that the angle of the leading lever arm is determined by the interaction between its own flexibility and the force exerted on it by the other head through their linkage, as illustrated in Figure 6B. Shortly after binding to actin, the leading head's active site presumably contains ADP or is empty, and if there were no intramolecular force between the heads, then the lever arm angle would still be directed toward the minus end of actin (dashed yellow lever), in a configuration similar to what we assumed for the trailing head. Such a scenario, however, would predict only one peak in the β distribution instead of the two peaks that we found. Because we detect the regular switching of β angles at the appropriate rate for the molecules' velocity (Figure 2 and Figure S3), we conclude that there is a large force between the two heads of the molecule. We hypothesize that the leading head is flexible (green segment in Figure 6B), possibly in the converter/unique insert region or at a ''pliant'' region at the base of one of the CaM subunits (Houdusse et al., 2000). Another likely compliant region in the molecule is the PTD (~80 residues after the CaM-bound IQ domain) that has been suggested to be unfolded on the basis of myosin VI's large step (Altman et al., 2004; Ökten et al., 2004; Rock et al., 2005). If these two compliances (stretching of the PTD and rotation of the leading head lever arm) are comparable, the strain would be partitioned between them and the leading lever arm would be bent backward as in Figure 6B (solid yellow lever). When a leading head binds to an actin monomer closer to the trailing head (cyan motor domain and lever), the smaller extension leads to a smaller $\beta_{leadinglever}$. Multiple actin binding sites thus result in multiple $\beta_{leadinglever}$ angles and the observed greater variance of $\beta_{leadingprobe}$ (Figure 3A). Our proposed role for strain in pulling the lever arm backward, and the consequent higher angular variability of the leading head compared to the trailing head, suggests that gating of the ATPase cycle would predominantly be exerted on the leading head (Sweeney and Houdusse, 2007). There are also implications of these ideas for changes in α, as described next.

Correlated Changes of α and β

If myosin VI simply walks straight with a ~180° power stroke rotation in the plane of actin (gray bar in Figure 6A and yellow leading head in Figure 6B), then the changes of β and α should be anticorrelated, i.e., when β_{probe} increases from 56° to 117° during the power stroke, α would decrease by ~60° and vice versa (Figure 6A). In addition to anticorrelation between $\Delta\beta$ and $\Delta\alpha$, we also observed correlation (both angles increase or decrease) between $\Delta\beta$ and $\Delta\alpha$ and noncorrelation (e.g., steps of β, without change of α) (see Table 1). The large variation of $\beta_{leadingprobe}$ (Figure 3A), $\Delta\alpha$ (Figure 3C), power stroke size (Altman et al., 2004; Rock et al., 2001), and step size (Ökten et al.,

2004; Park et al., 2006; Yildiz et al., 2004) of myosin VI all suggest large azimuthal flexibility of myosin VI that binds to widely varying actin monomers. For example, the sixth actin monomer along the short-pitch helix from a starting point is tipped 83° azimuthally rightward around actin, and the seventh monomer is tipped leftward −83°. The different types of $\Delta\beta$-$\Delta\alpha$ correlation in individual molecules (Table 1) suggest that both lever arms may flex or rotate to accommodate the azimuthal difference between the two heads.

As indicated in Figure 6A, steps giving changes of β less than 100° would be expected to be accompanied by $|\Delta\alpha|$ of less than 15°, so the much larger changes of α observed are indicative of large azimuthal motions of the head binding to different monomers along the actin helix. In a theoretical calculation by Lan and Sun (2006), the energy cost for myosin VI binding to monomers 6, 7, 9, and 11 are comparable, whether the stroke is either 12 or 20 nm. Lastly, molecules could differ from each other in the local probe orientation if some of the tightly bound CaM subunits at the unique insert exchanged with labeled CaM.

The Path of Myosin VI

After two steps of β, the lever arm should return to its former position, e.g., leading → trailing → leading. As explained in the Results, the probe azimuthal angle change, $^2\Delta\alpha$, after two consecutive steps indicates helical (two successive α changes occur in the same direction) or wiggly (successive α changes occur in opposite directions) motion irrespective of the relative orientation between the probe and the lever. The much broader width of the distribution of $^2\Delta\alpha$ values relative to $^2\Delta\beta$ (Figure 4) confirms that large azimuthal rotations are common, but α reverses its change (wiggles) more often than it changes twice in the same direction (Figure 4, bottom panels), contributing to a relatively straight overall path or gradual spiral. Strain in an extreme azimuthal step might introduce intramolecular torque, which would tend to restore the path in the following step.

The actin filaments in the single-molecule polTIRF experiments were attached rather firmly to the microscope slide by biotin-streptavidin linkages, probably restricting motions of the myosin VI molecules from squeezing between the filament and the slide. The broad and almost evenly distributed α angles (Figure 3B) imply that the molecules landed on the filaments over a broad range of angles and did not exhibit a strong preference for overall left-handed or right-handed motion.

In experiments designed to determine the path of myosin VI in the absence of physical restrictions around the actin filament, Ali et al. (2004) studied motions on actin filaments suspended away from the slide surface. In that geometry, 80% of the myosin VI molecules walked straight and 20% followed a right-handed helical path with a gradual pitch of 2.3 μm. Because the long-pitch helix of the actin filament is right handed, Ali et al. concluded that their results implied an even longer step than the 36 nm crossover distance of the two long-pitch strands. The twirling

experiments reported here, measuring the path of fila-
ments in a gliding assay, are compatible with Ali et al.'s re-
sults: many filaments went straight and ∼20% twirled with
a gradual right-handed helical motion (Figure 5). A right-
handed helical motion suggests that myosin VI leading
head binds actin monomer 6 or 15 more often than actin
monomer 7, 9, or 11. This relationship is energetically un-
favorable (Lan and Sun, 2006). However, if the rotation
plane of the power stroke is slightly tilted toward the right
side of the actin filament, the diffusive head would have
a better chance to bind actin monomer 6 and 15 than 7
and 11, thus causing a right-handed helical motion with
a long pitch.

Most of the time, myosin VI molecules walk in an overall
relatively straight path made up of chaotic left-right wig-
gling. The tilting motions measured here by polTIRF are
compatible with a surprisingly large (around 180°) rotation
during the power stroke, but other angles are produced
sometimes. When the heads bind to actin monomers at
markedly different azimuths, both of the lever arms seem
to be distorted, accommodating the extra intermolecular
stress. These features enable myosin VI to walk relatively
straight while sampling among several possible actin
binding sites.

The proximal tail domain and the postulated compliant
region between the motor domain and the lever arm junc-
tion provide great flexibility for motions and alternative
configurations of myosin VI binding to actin. Partition of
strain between the two compliances would lead to geom-
etries that vary the angle of the leading lever arms shown
in Figure 6 and allow biochemical gating of the leading
head for functional roles of processive transport and an-
choring (Buss et al., 2004; Sweeney and Houdusse,
2007). In cells, actin forms diverse structures such as par-
allel bundles and meshes. The flexible nature of myosin VI
that makes it possible to find several favorable binding
sites on single actin filaments presumably enables it to
bind to sites on two nearby filaments and thereby explore
pathways, routes, and anchoring positions on the diverse
actin structures in cells.

EXPERIMENTAL PROCEDURES

Preparation of Proteins

G-actin was obtained from rabbit skeletal muscle and purified as de-
scribed by Pardee and Spudich (1982). Biotinylated, Alexa 647-labeled
F-actin was prepared from G-actin, Alexa 647 actin (Molecular Probes,
Carlsbad, CA), and biotin-actin (Cytoskeleton, Denver, CO) at 1 μM
total actin monomer concentration with a ratio of 5:1:1 of G-actin:Alexa
647:biotin and stabilized with 1.1 μM phalloidin (Molecular Probes,
Carlsbad, CA). 0.3% rhodamine-labeled F-actin was prepared from
6′-IATR rhodamine-actin (Corrie and Craik, 1994) and stabilized with
1.1 μM phalloidin. The M6HMMsRod Myosin VI construct, a truncated
myosin VI with a fragment of smooth myosin II rod, was expressed in
SF9 cells and purified as described previously (Nishikawa et al.,
2002). This construct contains the mouse myosin VI sequence, resi-
dues Met1–Leu1023, including the motor domain, neck domain, and
coiled-coil domain, part of the chicken smooth muscle tail, residues
Gln1111–Asp1566, and a 6-His affinity tag. The portion of smooth

muscle rod ensures dimerization of the expressed myosin VI but is
too short to form filaments.

Residues Pro66 and Ala73 of chicken calmodulin (CaM) were
mutated to cysteine and labeled with bifunctional rhodamine (BR-I₂)
as described by Forkey et al. (2003). BR-I₂ was a generous gift from
Dr. J.E.T. Corrie (Corrie et al., 1998). Myosin VI was labeled by ex-
changing endogeneous CaM with exogenous BR-I₂-labeled mutant
CaM at low stoichiometry.

Buffers

M6BH buffer (pH = 7.6) contains 25 mM KCl, 20 mM HEPES, 2 mM
MgCl₂, and 1 mM EGTA in deionized water. M6BH⁺ buffer, the motility
buffer for single-molecule motility assays, is M6BH plus 10 mM dithio-
threitol (DTT) and 100 μg/ml wild-type CaM (WT-CaM, expressed in
bacteria as described by Putkey et al. [1985]). The motility buffer for
actin twirling assays is M6BH⁺ buffer plus 500–1000 μM ATP, 10 mM
phosphocreatine (Sigma P-7936), 0.3 mg/ml creatine phosphokinase
(prepared daily from powder, Sigma C3755), and 50 mM DTT.

Experimental Apparatus

In the single-molecule polTIRF setup described previously (Forkey
et al., 1999, 2000, 2003, 2005; Rosenberg et al., 2005), time multiplex-
ing between two incident paths, each polarized s and p relative to the
scattering plane, resulted in ambiguity of the deduced orientations out-
side one-eighth of a sphere. In the present work, time-multiplexed 45°
and 135° polarizations were added in each of the incident directions in
order to break these symmetries. Eight combinations of time-multi-
plexed incident directions and polarizations and two simultaneously
recorded emission intensities are accumulated in each 80 ms interval,
giving 16 different polarized fluorescence intensity traces (see
Figure S1 for details). This arrangement allows unambiguous 3D reso-
lution of individual probe dipoles within a hemisphere. With the current
setup, the average orientation of the probe during each 80 ms detec-
tion cycle is resolved to within ∼10°. Procedures for calibration and
data collection can be found in Beausang et al. (2007), Forkey et al.
(2003), Quinlan et al. (2005), and Rosenberg et al. (2005).

Single-Molecule Motility Assay

A precleaned fused silica slide (Quartz Scientific) was freshly treated
in an ion plasma cleaner for 5 min and spin coated with 2 mg/ml
poly(methyl methacrylate) (PMMA) (Aldrich Chemical, 37,003-7) in
methylene chloride. The PMMA-coated slide was assembled into
a 10–20 μl flow chamber with a glass coverslip and double-sided ad-
hesive tape. Actin was adhered to the surface and flow aligned with
the microscope x axis by successive incubations with 1 mg/ml biotiny-
lated BSA (Sigma, A-8549), 0.5 mg/ml streptavidin (Sigma, S-4762),
and 100 nM biotinylated, Alexa 647-labeled F-actin, each followed
by washes with M6BH⁺ buffer. Myosin VI, containing BR-labeled
CaM, was introduced into the sample chamber at 10–1000 pM in
M6BH⁺ and ATP as indicated.

Actin Twirling Assay

A flow chamber was assembled as above by using a glass coverslip
and a nitrocellulose-coated glass slide. Twenty microliters of
∼0.2 mg/ml unlabeled myosin VI was introduced into the sample
chamber and incubated for 2 min. Exposed nitrocellulose and fused
silica were blocked by 2 × 20 μl washes with 5 mg/ml BSA. 2 × 20 μl
of presheared, unlabeled F-actin was added in the absence of ATP
to block any inactive myosin heads, and excess actin was removed
by addition of M6BH⁺ buffer at 2 mM ATP, followed by two washes
of M6BH⁺ without ATP. Actin filaments, sparsely (0.3%) labeled with
rhodamine, were added in M6BH⁺ buffer, and then motility buffer
was added to initiate filament gliding and polTIRF measurements
were made of the rhodamine orientation.

REFERENCES

Ali, M.Y., Homma, K., Iwane, A.H., Adachi, K., Itoh, H., Kinosita, K., Jr., Yanagida, T., and Ikebe, M. (2004). Unconstrained steps of myosin VI appear longest among known molecular motors. Biophys. J. *86*, 3804–3810.

Altman, D., Sweeney, H.L., and Spudich, J.A. (2004). The mechanism of myosin VI translocation and its load-induced anchoring. Cell *116*, 737–749.

Bahloul, A., Chevreux, G., Wells, A.L., Martin, D., Nolt, J., Yang, Z., Chen, L.-Q., Potier, N., Van Dorsselaer, A., Rosenfeld, S., et al. (2004). The unique insert in myosin VI is a structural calcium-calmodulin binding site. Proc. Natl. Acad. Sci. USA *101*, 4787–4792.

Balci, H., Ha, T., Sweeney, H.L., and Selvin, P.R. (2005). Interhead distance measurements in myosin VI via SHRImP support a simplified hand-over-hand model. Biophys. J. *89*, 413–417.

Beausang, J.F., Schroeder, H.W., III, Gilmour, J.A., and Goldman, Y.E. (2006). Twirling of actin by myosins II and V. Biophys. J. *90*, 587a.

Beausang, J.F., Sun, Y., Quinlan, M.E., Forkey, J.N., and Goldman, Y.E. (2007). Single molecule fluorescence polarization via polarized total internal reflection fluorescent microscopy. In Laboratory Manual for Single Molecule Studies, P.R. Selvin and T. Ha, eds. (Cold Spring Harbor, NY: Cold Spring Harbor Laboratory Press).

Bryant, Z., Altman, D., and Spudich, J.A. (2007). The power stroke of myosin VI and the basis of reverse directionality. Proc. Natl. Acad. Sci. USA *104*, 772–777.

Buss, F., Spudich, G., and Kendrick-Jones, J. (2004). Myosin VI: cellular functions and motor properties. Annu. Rev. Cell Dev. Biol. *20*, 649–676.

Cheney, R.E., O'Shea, M.K., Heuser, J.E., Coelho, M.V., Wolenski, J.S., Espreafico, E.M., Forscher, P., Larson, R.E., and Mooseker, M.S. (1993). Brain myosin-V is a two-headed unconventional myosin with motor activity. Cell *75*, 13–23.

Corrie, J.E.T., and Craik, J.S. (1994). Synthesis and characterization of pure isomers of iodoacetamidotetramethylrhodamine. J. Chem. Soc. Perkin Trans. *1*, 2967–2973.

Corrie, J.E.T., Craik, J.S., and Munasinghe, V.R.N. (1998). A homobifunctional rhodamine for labeling proteins with defined orientations of a fluorophore. Bioconjug. Chem. *9*, 160–167.

Coureux, P.-D., Sweeney, H.L., and Houdusse, A. (2004). Three myosin V structures delineate essential features of chemo-mechanical transduction. EMBO J. *23*, 4527–4537.

Cramer, L.P. (2000). Myosin VI: roles for a minus end-directed actin motor in cells. J. Cell Biol. *150*, F121–F126.

De La Cruz, E.M., Ostap, E.M., and Sweeney, H.L. (2001). Kinetic mechanism and regulation of myosin VI. J. Biol. Chem. *276*, 32373–32381.

Dominguez, R., Freyzon, Y., Trybus, K.M., and Cohen, C. (1998). Crystal structure of a vertebrate smooth muscle myosin motor domain and its complex with the essential light chain: visualization of the pre-power stroke state. Cell *94*, 559–571.

Forkey, J.N., Quinlan, M.E., Corrie, J.E.T., and Goldman, Y.E. (1999). Single-molecule structural dynamics by fluorescence polarization microscopy. Biophys. J. *76*, A20.

Forkey, J.N., Quinlan, M.E., and Goldman, Y.E. (2000). Protein structural dynamics by single-molecule fluorescence polarization. Prog. Biophys. Mol. Biol. *74*, 1–35.

Forkey, J.N., Quinlan, M.E., Shaw, M.A., Corrie, J.E.T., and Goldman, Y.E. (2003). Three-dimensional structural dynamics of myosin V by single-molecule fluorescence polarization. Nature *422*, 399–404.

Forkey, J.N., Quinlan, M.E., and Goldman, Y.E. (2005). Measurement of single macromolecule orientation by total internal reflection fluorescence polarization microscopy. Biophys. J. *89*, 1261–1271.

Frank, D.J., Noguchi, T., and Miller, K.G. (2004). Myosin VI: a structural role in actin organization important for protein and organelle localization and trafficking. Curr. Opin. Cell Biol. *16*, 189–194.

Hasson, T. (2003). Myosin VI: two distinct roles in endocytosis. J. Cell Sci. *116*, 3453–3461.

Hasson, T., and Mooseker, M.S. (1994). Porcine myosin-VI: characterization of a new mammalian unconventional myosin. J. Cell Biol. *127*, 425–440.

Houdusse, A., Szent-Györgyi, A.G., and Cohen, C. (2000). Three conformational states of scallop myosin S1. Proc. Natl. Acad. Sci. USA *97*, 11238–11243.

Howard, J. (1997). Molecular motors: structural adaptations to cellular functions. Nature *389*, 561–567.

Iwaki, M., Tanaka, H., Iwane, A.H., Katayama, E., Ikebe, M., and Yanagida, T. (2006). Cargo-binding makes a wild-type single-headed myosin-VI move processively. Biophys. J. *90*, 3643–3652.

Kerssemakers, J.W.J., Munteanu, E.L., Laan, L., Noetzel, T.L., Janson, M.E., and Dogterom, M. (2006). Assembly dynamics of microtubules at molecular resolution. Nature *442*, 709–712.

Lan, G., and Sun, S.X. (2006). Flexible light-chain and helical structure of F-actin explain the movement and step size of myosin-VI. Biophys. J. *91*, 4002–4013.

Lister, I., Schmitz, S., Walker, M., Trinick, J., Buss, F., Veigel, C., and Kendrick-Jones, J. (2004). A monomeric myosin VI with a large working stroke. EMBO J. *23*, 1729–1738.

Mehta, A.D., Rock, R.S., Rief, M., Spudich, J.A., Mooseker, M.S., and Cheney, R.E. (1999). Myosin-V is a processive actin-based motor. Nature *400*, 590–593.

Ménétrey, J., Bahloul, A., Wells, A.L., Yengo, C.M., Morris, C.A., Sweeney, H.L., and Houdusse, A. (2005). The structure of the myosin VI motor reveals the mechanism of directionality reversal. Nature *435*, 779–785.

Ménétrey, J., Llinas, P., Mukherjea, M., Sweeney, H.L., and Houdusse, A. (2007). The structural basis for the large powerstroke of myosin VI. Cell *131*, 300–308.

Morris, C.A., Wells, A.L., Yang, Z., Chen, L.-Q., Baldacchino, C.V., and Sweeney, H.L. (2003). Calcium functionally uncouples the heads of myosin VI. J. Biol. Chem. *278*, 23324–23330.

Nishikawa, S., Homma, K., Komori, Y., Iwaki, M., Wazawa, T., Iwane, A.H., Saito, J., Ikebe, R., Katayama, E., Yanagida, T., and Ikebe, M. (2002). Class VI myosin Moves processively along actin filaments backward with large steps. Biochem. Biophys. Res. Commun. *290*, 311–317.

Ökten, Z., Churchman, L.S., Rock, R.S., and Spudich, J.A. (2004). Myosin VI walks hand-over-hand along actin. Nat. Struct. Mol. Biol. *11*, 884–887.

Otterbein, L.R., Graceffa, P., and Dominguez, R. (2001). The crystal structure of uncomplexed actin in the ADP state. Science *293*, 708–711.

Pardee, J.D., and Spudich, J.A. (1982). Purification of muscle actin. Methods Cell Biol. *24*, 271–289.

Park, H., Ramamurthy, B., Travaglia, M., Safer, D., Chen, L.-Q., Franzini-Armstrong, C., Selvin, P.R., and Sweeney, H.L. (2006). Full-length myosin VI dimerizes and moves processively along actin filaments upon monomer clustering. Mol. Cell *21*, 331–336.

Park, H., Li, A., Chen, L.-Q., Houdusse, A., Selvin, P.R., and Sweeney, H.L. (2007). The unique insert at the end of the myosin VI Motor is the sole determinant of directionality. Proc. Natl. Acad. Sci. USA *104*, 778–783.

Purcell, T.J., Morris, C., Spudich, J.A., and Sweeney, H.L. (2002). Role of the lever arm in the processive stepping of myosin V. Proc. Natl. Acad. Sci. USA *99*, 14159–14164.

Putkey, J.A., Slaughter, G.R., and Means, A.R. (1985). Bacterial expression and characterization of proteins derived from the chicken calmodulin cDNA and a calmodulin processed gene. J. Biol. Chem. *260*, 4704–4712.

Quinlan, M.E., Forkey, J.N., and Goldman, Y.E. (2005). Orientation of the myosin light chain region by single molecule total internal reflection fluorescence polarization microscopy. Biophys. J. *89*, 1132–1142.

Rayment, I., Holden, H.M., Whittaker, M., Yohn, C.B., Lorenz, M., Holmes, K.C., and Milligan, R.A. (1993). Structure of the actin-myosin complex and its implications for muscle contraction. Science *261*, 58–65.

Robblee, J.P., Olivares, A.O., and De La Cruz, E.M. (2004). Mechanism of nucleotide binding to actomyosin VI. J. Biol. Chem. *279*, 38608–38617.

Rock, R.S., Rice, S.E., Wells, A.L., Purcell, T.J., Spudich, J.A., and Sweeney, H.L. (2001). Myosin VI is a processive motor with a large step size. Proc. Natl. Acad. Sci. USA *98*, 13655–13659.

Rock, R.S., Ramamurthy, B., Dunn, A.R., Beccafico, S., Rami, B.R., Morris, C., Spink, B.J., Franzini-Armstrong, C., Spudich, J.A., and Sweeney, H.L. (2005). A flexible domain is essential for the large step size and processivity of myosin VI. Mol. Cell *17*, 603–609.

Rosenberg, S.A., Quinlan, M.E., Forkey, J.N., and Goldman, Y.E. (2005). Rotational motions of macromolecules by single-molecule fluorescence microscopy. Acc. Chem. Res. *38*, 583–593.

Smith, C.A,, and Rayment, I. (1996). X-ray structure of the magnesium(II)-.ADP.vanadate complex of the Dictyostelium discoideum myosin motor domain to 1.9 Å resolution. Biochemistry *35*, 5404–5417.

Sweeney, H.L., and Houdusse, A. (2007). What can myosin VI Do in cells? Curr. Opin. Cell Biol. *19*, 57–66.

Syed, S., Snyder, G.E., Franzini-Armstrong, C., Selvin, P.R., and Goldman, Y.E. (2006). Adaptability of myosin V studied by simultaneous detection of position and orientation. EMBO J. *25*, 1795–1803.

Tyska, M.J., and Warshaw, D.M. (2002). The myosin power stroke. Cell Motil. Cytoskeleton *51*, 1–15.

Walker, M.L., Burgess, S.A., Sellers, J.R., Wang, F., Hammer, J.A., III, Trinick, J., and Knight, P.J. (2000). Two-headed binding of a processive myosin to F-actin. Nature *405*, 804–807.

Wells, A.L., Lin, A.W., Chen, L.-Q., Safer, D., Cain, S.M., Hasson, T., Carragher, B.O., Milligan, R.A., and Sweeney, H.L. (1999). Myosin VI is an actin-based motor that moves backwards. Nature *401*, 505–508.

Yildiz, A., and Selvin, P.R. (2005). Fluorescence imaging with one nanometer accuracy: application to molecular motors. Acc. Chem. Res. *38*, 574–582.

Yildiz, A., Forkey, J.N., McKinney, S.A., Ha, T., Goldman, Y.E., and Selvin, P.R. (2003). Myosin V walks hand-over-hand: single fluorophore imaging with 1.5-nm localization. Science *300*, 2061–2065.

Yildiz, A., Park, H., Safer, D., Yang, Z., Chen, L.-Q., Selvin, P.R., and Sweeney, H.L. (2004). Myosin VI steps via a hand-over-hand mechanism with its lever arm undergoing fluctuations when attached to actin. J. Biol. Chem. *279*, 37223–37226.